Supporting Information for

Reactant Conversion-Intercalation Strategy toward Interlayer-expanded MoS_2 Microflowers with Superior Supercapacitor Performance

Jingwei Wang,[a] Xuejun Zheng,*[a] Yaoyong Dong,[a] Longyuan Chen,[a] Lijuan Chen,[a] Wenyuan He,*[a,b]

[a] *School of Mechanical Engineering and Mechanics, Xiangtan University, Xiangtan, 411105, China*

[b] *Research Institute of Green Intelligent Manufacturing, Xiangtan University, Foshan 528399, China.*

*Corresponding authors:

E-mail address: zhengxuejun@xtu.edu.cn; hewenyuan@xtu.edu.cn.

Details of the electrochemical measurements

In the three-electrode setup, the active materials coated on Ni foam current collectors were served as the work electrode, Ni foam plate as the counter electrode, saturated calomel electrode (SCE) as the reference electrode and 1 M sodium sulfate (Na_2SO_4) as the electrolyte. A Luggin capillary was employed to control the placement of the reference electrode relative to the working electrode. The working electrodes were fabricated by mixing active materials, acetylene black, polyvinylidene fluoride (PVDF) in a weight ratio of 8: 1: 1, using N-methyl-2-pyrrolidone (NMP) as the solvent. The mixed slurry was pressed onto Ni foam current collectors (1 cm^2), followed by drying in a vacuum oven at 100 °C for 12 h, and the mass loading of the electrode materials was controlled to be about 6~8 mg. The cyclic voltammetry (CV) curves at the scan rates of 5~100 mV s^{-1} and galvanostatic charge-discharge (GCD) curves at the current densities of 0.5~5 A g^{-1} were collected in the potential rage of −1.0~−0.3 V. The electrochemical impedance spectroscopy (EIS) was recorded in the frequency range from 0.01 kHz to 100 kHz at the open-circuit potential with the amplitude of 5 mV. Cyclic stability was characterized using GCD measurements over 3000 cycles at a current density of 2 A g^{-1}. The mass specific capacitance could also be calculated from their CV and GCD by the following formulas [1]:

$$C = \frac{\int IdV}{\nu m \Delta V} \quad (1)$$

$$C = \frac{I \Delta t}{m \Delta V} \quad (2)$$

Where C is the specific capacitance (F g^{-1}), I is current (A), ν is the scan rate (mV s^{-1}), m is the weight of active materials (g), ΔV is the range of potential windows (V), Δt is the discharge time (s).

The button-type symmetric supercapacitor (BSSC) was assembled by the two as-fabricated equal

working electrodes and glass fiber separator immersed by 1 M Na_2SO_4 electrolyte. After assembling the supercapacitor configuration, the assembled device needs to stand for more than 12 hours to make electrolyte homogeneously diffuse into the electrodes. CV curves at the scan rates from 5 to 100 mV s^{-1} and GCD curves at the current densities from 0.5 to 5 A g^{-1} were recorded in the potential range of 0~1.2 V for the BSSC. The stability of the BSSC was also estimated by cyclic performance for 3000 cycles at the current density of 2 A g^{-1}. The capacitance of single electrode (C_T, F g^{-1}) based on the CV curves for the BSSC was calculated using the equation (3). Based on the GCD curves, the capacitance of single electrode (C_{Tg}, F g^{-1}), energy density (E, Wh kg^{-1}) and power density (P, W kg^{-1}) of the BSSC were calculated using the following equations (4), (5) and (6), respectively [2]:

$$C_T = \frac{4\int IdV}{vm\Delta V} \quad (3)$$

$$C_{Tg} = \frac{4I\Delta t}{m\Delta V} \quad (4)$$

$$E = \frac{C_{Tg}(\Delta V)^2}{8\times 3.6} \quad (5)$$

$$P = \frac{E\times 3600}{T_{discharge}} \quad (6)$$

where m is the total mass of active materials in both anode and cathode (g), ΔV is the working potential window, $T_{discharge}$ is the discharging time (s).

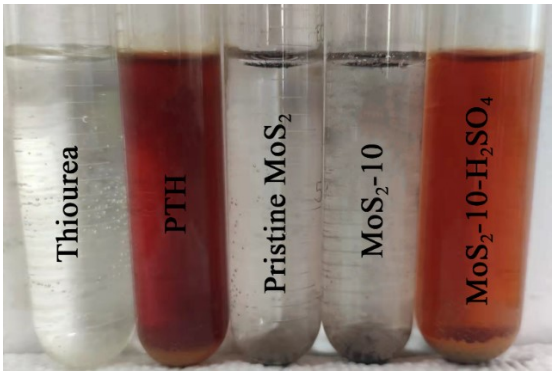

Fig. S1 Photograph of the thiourea, PTH, pristine MoS_2, MoS_2-10 aqueous dispersions and MoS_2-10

dilute sulfuric acid dispersion (MoS_2-10-H_2SO_4) after adding ferric sulfate.

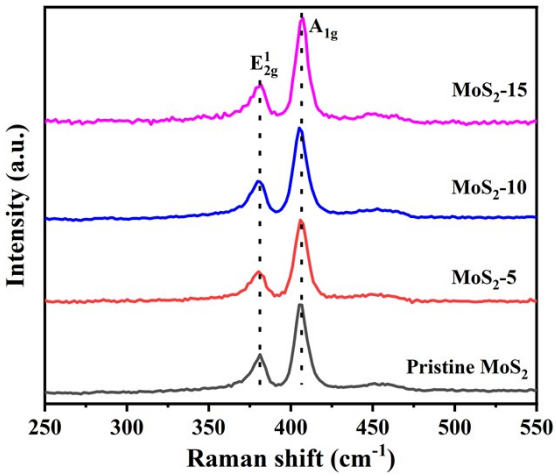

Fig. S2 Raman spectra of the pristine MoS_2 and E-MoS_2.

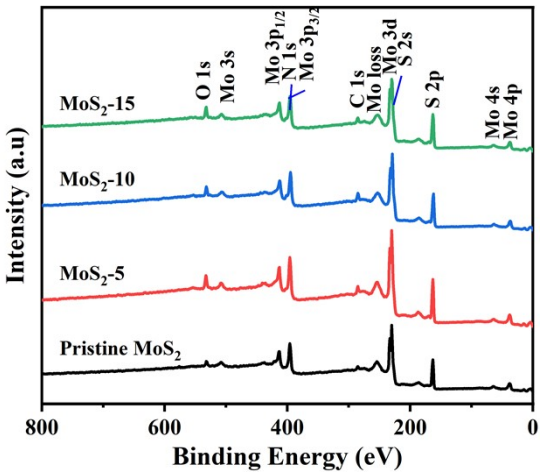

Fig. S3 XPS survey spectra of the pristine MoS_2 and E-MoS_2.

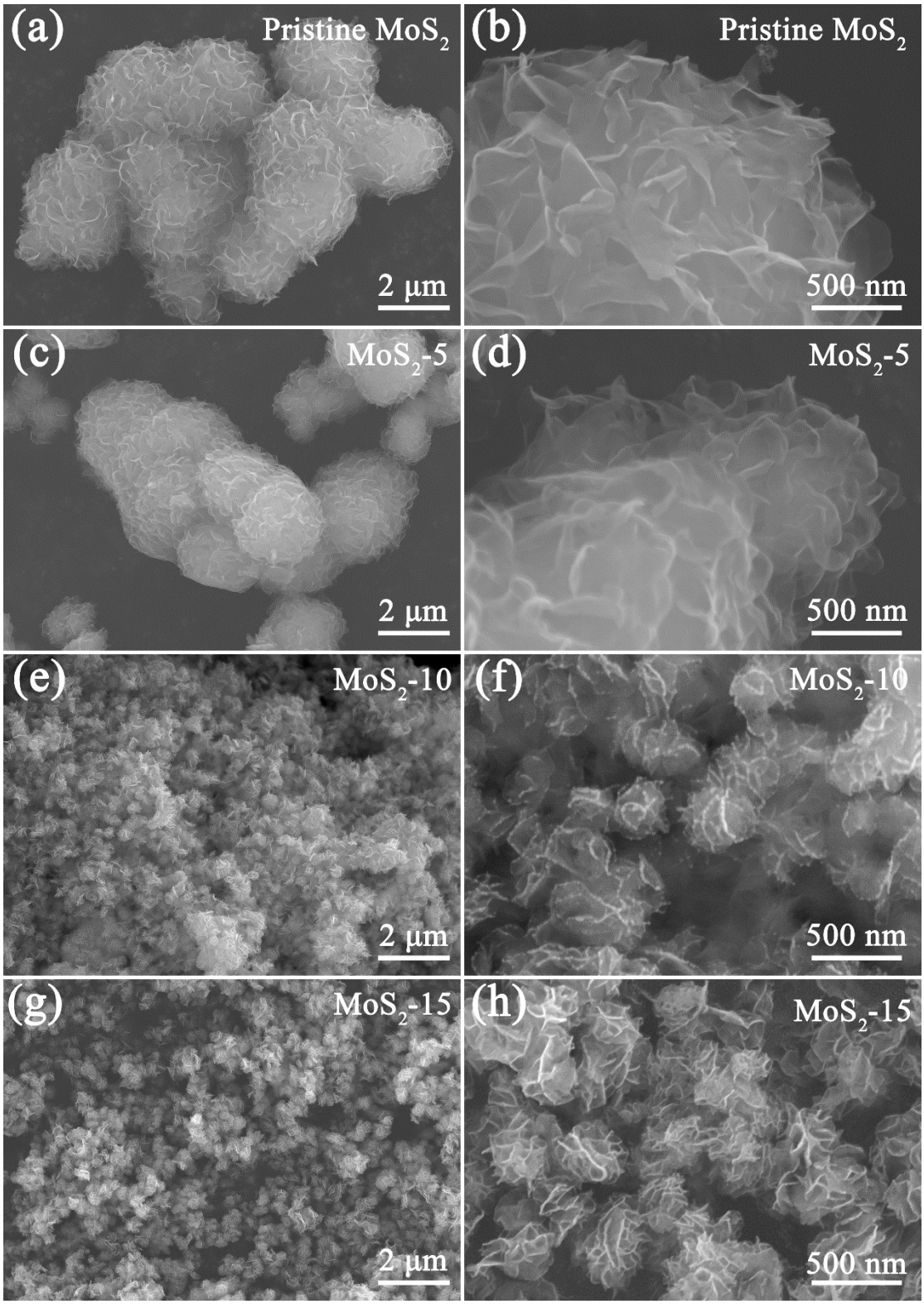

Fig. S4 Field-emission scanning electron microscope (FESEM) images for the (a) pristine MoS_2, (c) MoS_2-5, (e) MoS_2-10, and (g) MoS_2-15 in low magnification and the (b) pristine MoS_2, (d) MoS_2-5, (f) MoS_2-10, and (h) MoS_2-15 in high magnification.

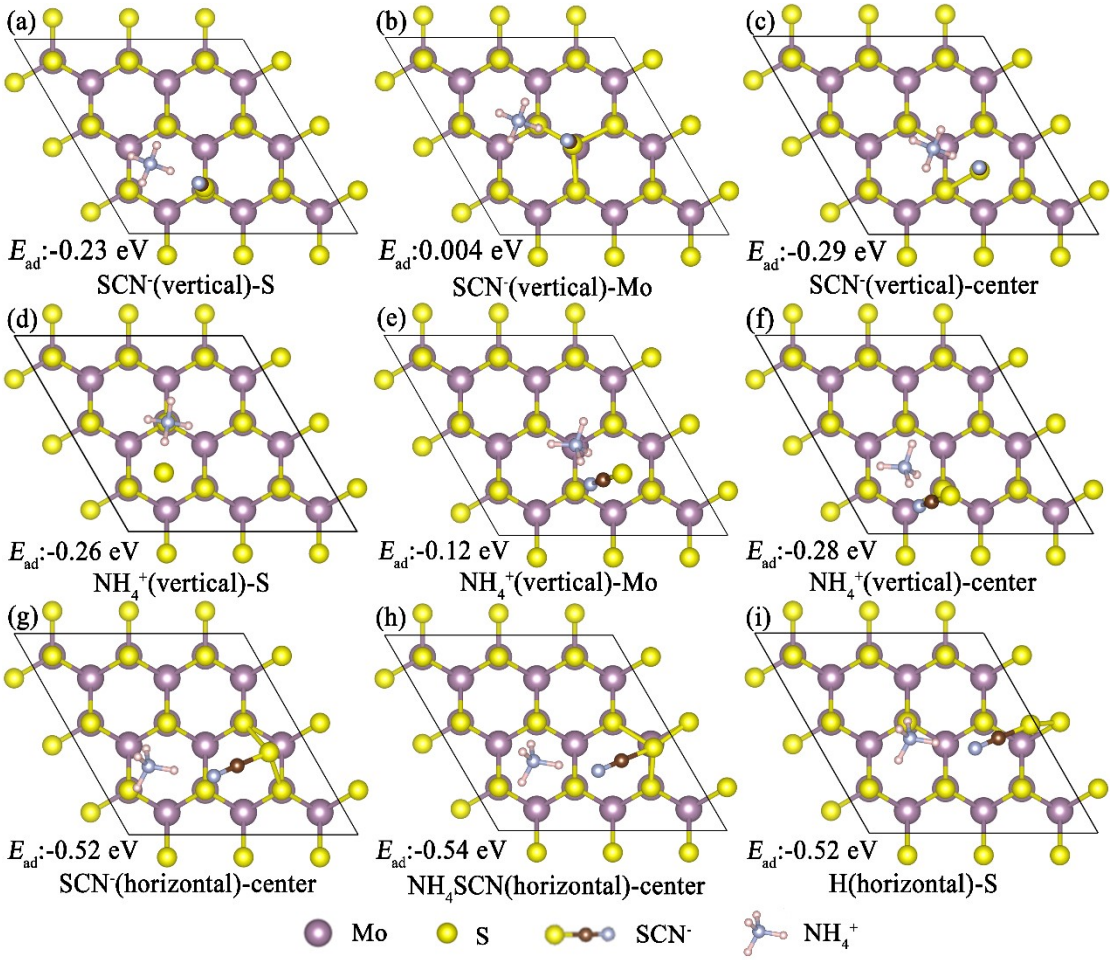

Fig. S5 Top view for the adsorption sites and the corresponding adsorption energies (E_{ad}) of NH_4^+ and SCN^- on the MoS_2 nanosheet. (a) SCN^-(vertical)-S; (b) SCN^-(vertical)-Mo; (c) SCN^-(vertical)-center; (d) NH_4^+(vertical)-Mo; (e) NH_4^+(vertical)-S; (f) NH_4^+(vertical)-center; (g) SCN^-(horizontal)-center; (h) NH_4SCN (horizontal)-center; (i) H(horizontal)-S.

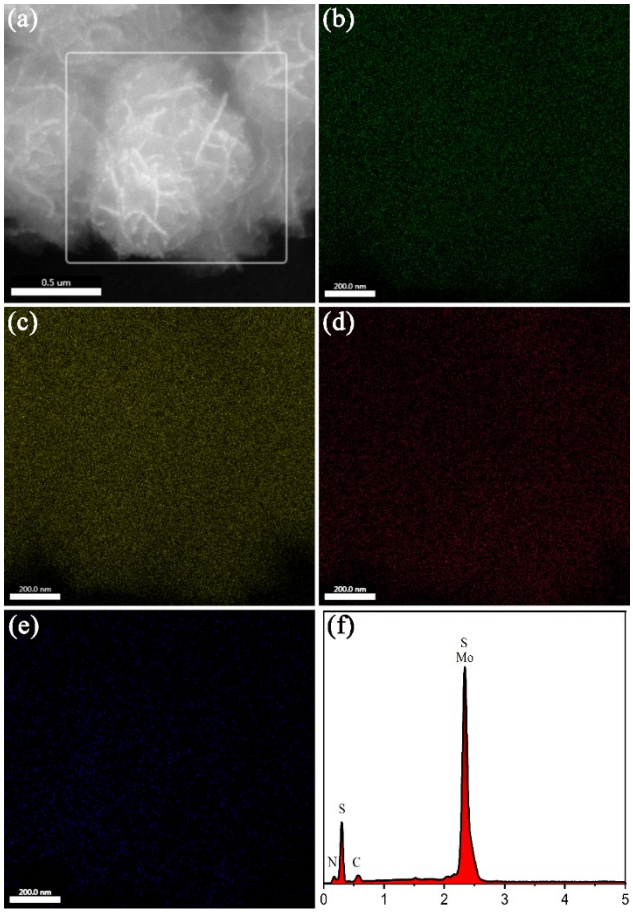

Fig. S6 The element mapping images of the MoS_2-10.

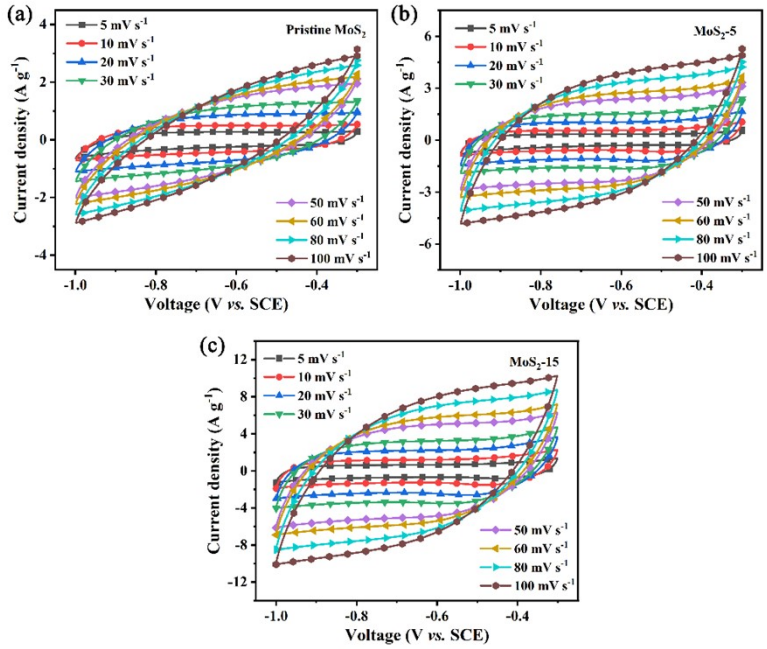

Fig. S7 CV curves of (a) the pristine MoS_2, (b) MoS_2-5 and (c) MoS_2-15 at various scan rates in three electrodes system.

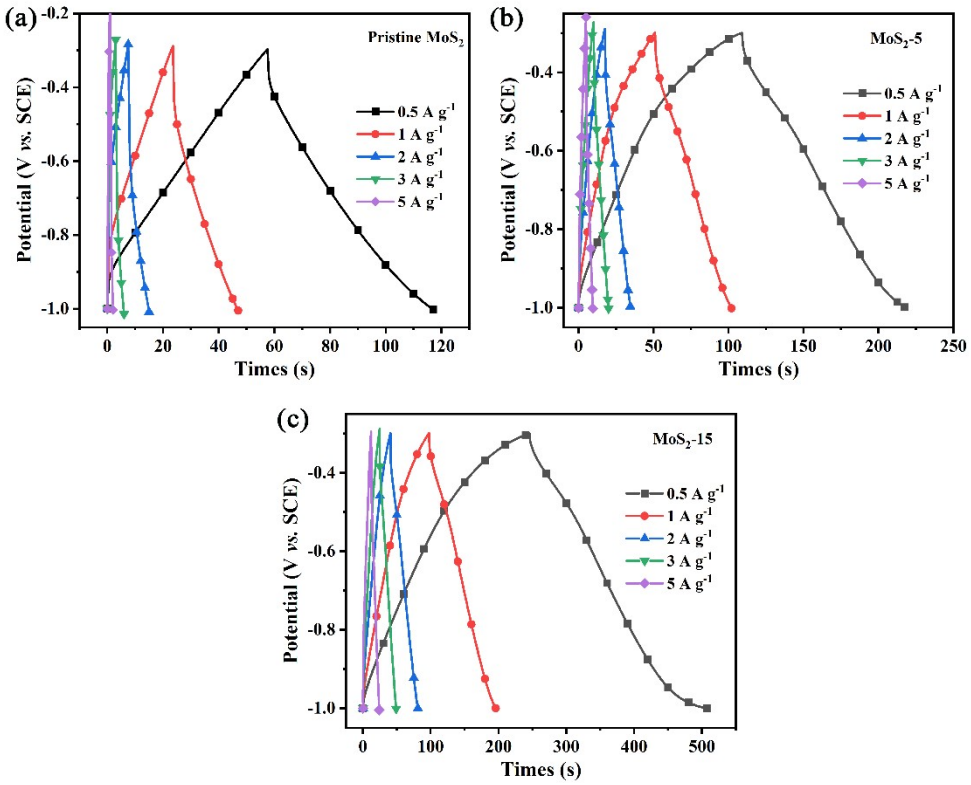

Fig. S8. GCD curves of (a) the pristine MoS_2, (b) MoS_2-5 and (c) MoS_2-15 at various current densities in three electrodes system.

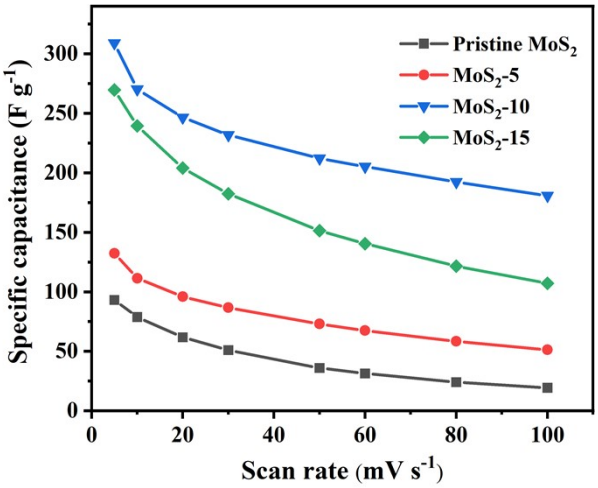

Fig. S9 Specific capacitance derived from CV curves for the pristine MoS_2 and E-MoS_2 at various scan rates in three electrodes system.

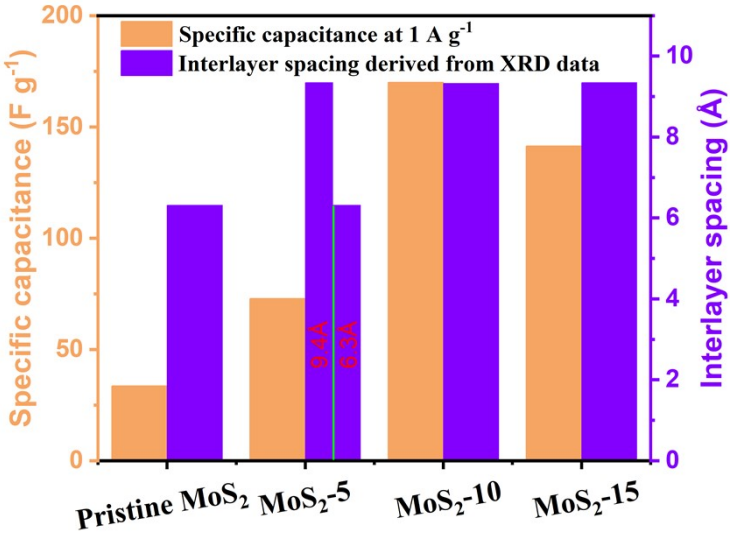

Fig. S10 The relationship between the specific capacitance and the interlayer spacing for the pristine MoS_2 and E-MoS_2 microflowers in three electrodes system.

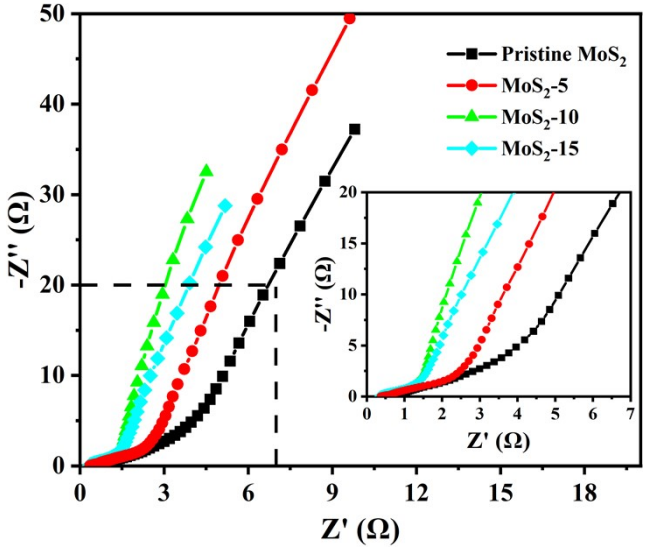

Fig. S11 Nyquist plots of the pristine MoS_2 and E-MoS_2 at open circuit voltage in three electrodes system.

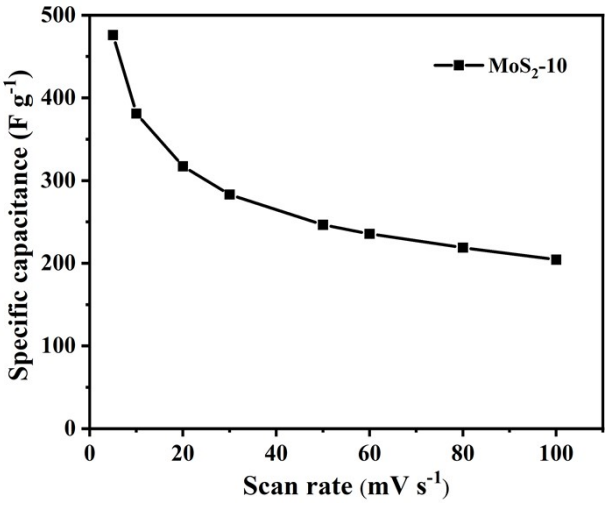

Fig. S12 Specific capacitance of the symmetric supercapacitor based on MoS_2-10 electrode at various scan rates.

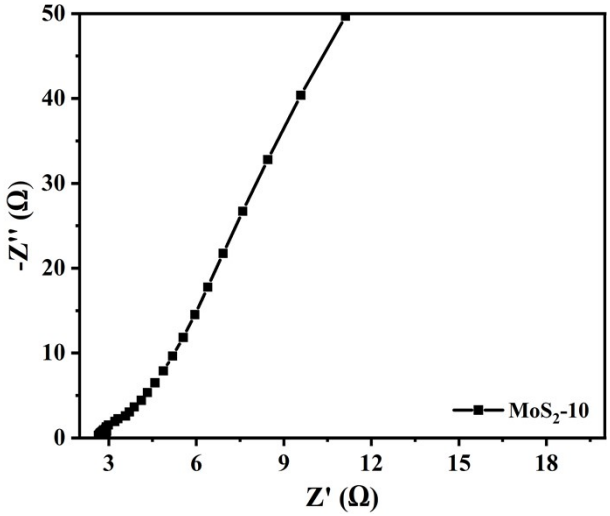

Fig. S13. Nyquist plots of symmetric supercapacitor based on MoS_2-10 electrode at open circuit voltage.

Table. S1 Comparison of electrochemical performance with other reports.

Materials	Electrolyte	Capacitance (three electrodes system)	Capacitance (symmetric supercapacitor)	Energy density	Power density	Ref.
MoS_2@CC	LiCl-PVA	--	368 F g^{-1} at 5 mV s^{-1}	5.42	128	3
MoS_2/PPY	1 M H_2SO_4	--	400 F g^{-1} at 1 A g^{-1}	2.6	212	4
MoS_2/TiO_2/ Ti	PVA-H_3PO_4	--	230.24 F g^{-1} at 5 mV s^{-1}	2.7	530.9	5
1T/2H MoS_2	0.5 M K_2SO_4	208 F g^{-1} at 0.5 A g^{-1}	37.2 F g^{-1} at 0.5 A g^{-1}	4.19	225	6
EO&IE MoS_2/rGO	HCl	143.2 F g^{-1} at 50 mV s^{-1}	--	--	--	7
sphere like MoS_2	1 M Na_2SO_4	92.85 F g^{-1} at 0.5 mA cm^{-2}	--	7.25	186.5	8
E-MoS_2	1 M Na_2SO_4	246.8.0 F g^{-1} at 0.5 A g^{-1}	263.33 F g^{-1} at 0.5 A g^{-1}	7.33	1200	this work

References

1 M. Acerce, D. Voiry, M. Chhowalla, *Nat. Nanotechnol.*, 2015, **10**, 313-318.

2 P. Wang, G. Zhang, M. Li, Y. Yin, J. Li, G. Li, W. Wang, W. Peng, F. Cao, Y. Guo, *Chem. Eng. J.*, 2019, **375**, 122020.

3 M.S. Javed, S. Dai, M. Wang, D. Guo, L. Chen, X. Wang, C. Hu, Y. Xi, *J. Power Sources*, 2015, **285**, 63-69.

4 A.K. Thakur, R.B. Choudhary, M. Majumder, G. Gupta, M. Shelke, *J. Electroanal. Chem.*, 2016, **782**, 278-287.

5 X. Li, X. Li, J. Cheng, D. Yuan, W. Ni, Q. Guan, L. Gao, B. Wang, *Nano Energy*, 2016, **21**, 228-237.

6 B.A. Ali, A.M.A. Omar, A.S.G. Khalil, N.K. Allam, *ACS Appl. Mater. Interfaces*, 2019, **11**, 33955-33965.

7 Y. Ji, Q. Wei, Y. Sun, *Ind. Eng. Chem. Res.*, 2018, **57**, 4571-4576.

8 K. Krishnamoorthy, G.K. Veerasubramani, S. Radhakrishnan, S.J. Kim, *Mater. Res. Bull.*, 2014, **50**, 499-502.